

Semi-Supervised Semantic Segmentation with Professional and General Training

Yuting Hong¹, Hui Xiao¹, Huazheng Hao¹, Xiaojie Qiu², Baochen Yao¹,
Chengbin Peng^{1*}

¹Faculty of Electrical Engineering and Computer Science, Ningbo University, Ningbo, 315200, China.

²Zhejiang Cowain Automation Technology Co., Ltd., Ningbo, 315200, China.

*Corresponding author(s). E-mail(s): pengchengbin@nbu.edu.cn;

Abstract

With the advancement of convolutional neural networks, semantic segmentation has achieved remarkable progress. The training of such networks heavily relies on image annotations, which are very expensive to obtain. Semi-supervised learning can utilize both labeled data and unlabeled data with the help of pseudo-labels. However, in many real-world scenarios where classes are imbalanced, majority classes often play a dominant role during training and the learning quality of minority classes can be undermined. To overcome this limitation, we propose a synergistic training framework, including a professional training module to enhance minority class learning and a general training module to learn more comprehensive semantic information. Based on a pixel selection strategy, they can iteratively learn from each other to reduce error accumulation and coupling. In addition, a dual contrastive learning with anchors is proposed to guarantee more distinct decision boundaries. In experiments, our framework demonstrates superior performance compared to state-of-the-art methods on benchmark datasets.

Keywords: Semi-Supervised Learning, Semantic Segmentation, Contrastive Learning

1 Introduction

Semantic segmentation, a critical task in computer vision, involves assigning a specific label to each pixel [1–3]. This pixel-level classification problem is notably more complex than image classification [4] or object detection [5] in the field of computer vision. Many approaches to semantic segmentation utilize an encoder-decoder architecture [6, 7], a strategy often employed in fields such as defect detection and autonomous driving. The dependence of supervised learning techniques on large-scale, accurately annotated datasets, which

are often costly to produce, has sparked considerable interest in leveraging weakly labeled, easily labeled, and unlabeled data to boost model performance [8–13]. Specifically, there has been significant progress in semi-supervised semantic segmentation, which combines a small amount of labeled data with a large volume of unlabeled data.

Semi-supervised semantic segmentation methods generally revolve around three core architectures: mean teacher [14, 15, 17], cross confidence consistency [16], and cross pseudo supervision [11], as illustrated in Fig. 1. In mean teacher

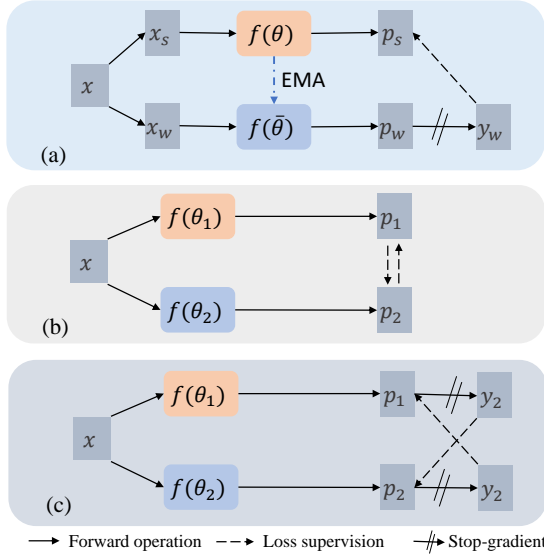


Fig. 1: Illustration of some architectures. (a) Mean teacher [14, 15] with a teacher model $f(\theta)$ and a student model $f(\bar{\theta})$. (b) Cross confidence consistency [16] with two student models $f(\theta_1)$ and $f(\theta_2)$. (c) Cross pseudo supervision [11] with two student models $f(\theta_1)$ and $f(\theta_2)$. x_w , x_s denote the samples with weak and strong augmentation, respectively.

architecture, the teacher model functions as an exponential moving average (EMA) of the student model [18], as depicted in Fig. 1(a). The other two architectures involve two student models with the same architecture learning from each other, as shown in Fig. 1(b) and Fig. 1(c). Additionally, two primary learning strategies are employed in semi-supervised semantic segmentation: consistency regularization [19–21] and entropy minimization [22–24]. Consistency regularization guarantees that a classifier generates similar predictions for a sample when subjected to various perturbations, and entropy minimization is a self-training process where a model is supervised using pseudo-labels generated by another model.

However, these approaches do not pay attention to class imbalance issues, and most of them are likely to suffer from model coupling issues [18, 25], both of which can lead to more severe error accumulation. To overcome these limitations, we propose a **Synergistic Training** framework with **Professional** and **General Training** (STPG), as shown in Fig. 2. The simple yet effective framework consists of two modules: a professional

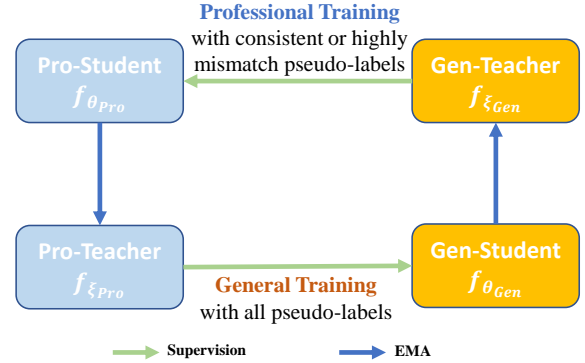


Fig. 2: Illustration of the synergistic training framework. It contains a Gen-Student with a corresponding Gen-Teacher and a Pro-Student with a corresponding Pro-Teacher. Pro-Student acquires knowledge from Gen-Teacher to focus on high-quality and highly mismatched pseudo-labels and then transfers knowledge to Pro-Teacher. Gen-Student is supervised by all pseudo-labels from Pro-Teacher to obtain more comprehensive semantic information and then transfers knowledge to Gen-Teacher. Through loopy updates, high-quality and difficult samples can be continuously learned.

training module and a general training module. The first module only selects pseudo-labels that are predicted consistently or highly mismatched between a professional student (Pro-Student) and a general teacher (Gen-Teacher), which can learn more minority class information and reduce error accumulation. In the second module, a general student (Gen-Student) is supervised by all pseudo-labels from a professional teacher (Pro-Teacher), which can learn more comprehensive semantic information. As the two modules are different, they are unlikely to be coupled. To our knowledge, this method represents a pioneering approach in semi-supervised semantic segmentation, addressing both class imbalance and model coupling issues simultaneously.

Our contributions are summarized as follows:

- We propose a synergistic training framework with professional and general training modules, which promotes the learning of high-quality and minority-class pixels and reduces the influence of unreliable pseudo-labels.

- To further improve the learning of minority classes, we propose dual contrastive learning with anchors which can highlight decision boundaries between different classes.
- We demonstrate that our approach significantly boosts the model performance and outperforms the state-of-the-art techniques on two well-established datasets.

2 Related Work

Semantic Segmentation plays a crucial role in computer vision, serving as a cornerstone for numerous applications. Recent advancements have witnessed remarkable strides in semantic segmentation, which are largely propelled by deep convolutional neural networks (CNNs) [26] and transformers [27]. The leading-edge approaches in semantic segmentation [28–30] predominantly adhere to the encoder-decoder paradigm [7]. In this paradigm, the decoder replaces fully connected layers that are typically employed in classification tasks with convolutional layers, enabling pixel-wise predictions. However, conventional supervised approaches heavily depend on large-scale, precisely annotated datasets, which can be prohibitively expensive to acquire in practice.

Semi-Supervised Learning has seen significant advancements in recent years. Many of these methods share similar basic techniques, such as consistency regularization [31–33] or pseudo-labeling [34, 35]. Consistency regularization is based on the clustering assumption that a decision boundary typically passes through a region with low sample density; thus, predictions are consistent under perturbations. Pseudo-labeling is based on the natural idea that predictions obtained from a model can be reused as supervision, which is motivated by entropy minimization. For example, FixMatch [24] is notable for its technique of generating pseudo-labels from weakly augmented unlabeled images and utilizing them to supervise models fed with strongly augmented images. Long-tail distribution has been extensively studied in semi-supervised learning. DST [36] enhances the quality of pseudo-labels by adversarially optimizing representations to avoid worst-case scenarios. BaCon [37] employs a meticulously crafted contrastive approach to directly regularize the distribution of instance representations.

Semi-Supervised Semantic Segmentation aims to utilize both unlabeled data and labeled data to train a high-performance segmentation network that can assign pseudo-labels to images. Due to limited labeled data, the full utilization of unlabeled data has become an important issue. Preliminary works have focused on consistency regularization and entropy minimization. U²PL [15] uses unreliable data for contrastive learning to boost performance. PRCL [38] introduces a framework that enhances representation quality by incorporating its probability. MMFA [39] introduces a framework for feature augmentation that incorporates both multi-reliability and multi-level strategies to fully exploit pixel information. CTT [25] alleviates model coupling issues through dual mean teacher architecture. Recently, numerous contrastive learning methods [40, 41] have been proposed for semi-supervised semantic segmentation. However, the above semi-supervised semantic segmentation methods do not sufficiently explore the semantic information within minority classes. In this manuscript, we propose a synergistic training framework with two training modules and a dual contrastive learning to resolve class imbalance issues.

3 Method

In this section, first, we define the problem. Second, we introduce the synergistic training framework. Last, we describe the utilization of dual contrastive learning with anchors.

3.1 Problem Definition

Let \mathcal{D} be a dataset that consists of a labeled set $\mathcal{D}_l = \{(x_l^i, y_l^i)\}_{i=1}^{N_l}$ and an unlabeled set $\mathcal{D}_u = \{(x_u^i)\}_{i=1}^{N_u}$, where x^i is an input image and y^i represents the corresponding pixel-level ground-truth. N_l and N_u denote the numbers of labeled images and unlabeled images, respectively, and generally $N_l \ll N_u$. In our approach, labeled data and unlabeled data are sampled equally in each training process. Our objective is to construct an effective semantic segmentation model by integrating a substantial quantity of unlabeled data with a small portion of labeled data.

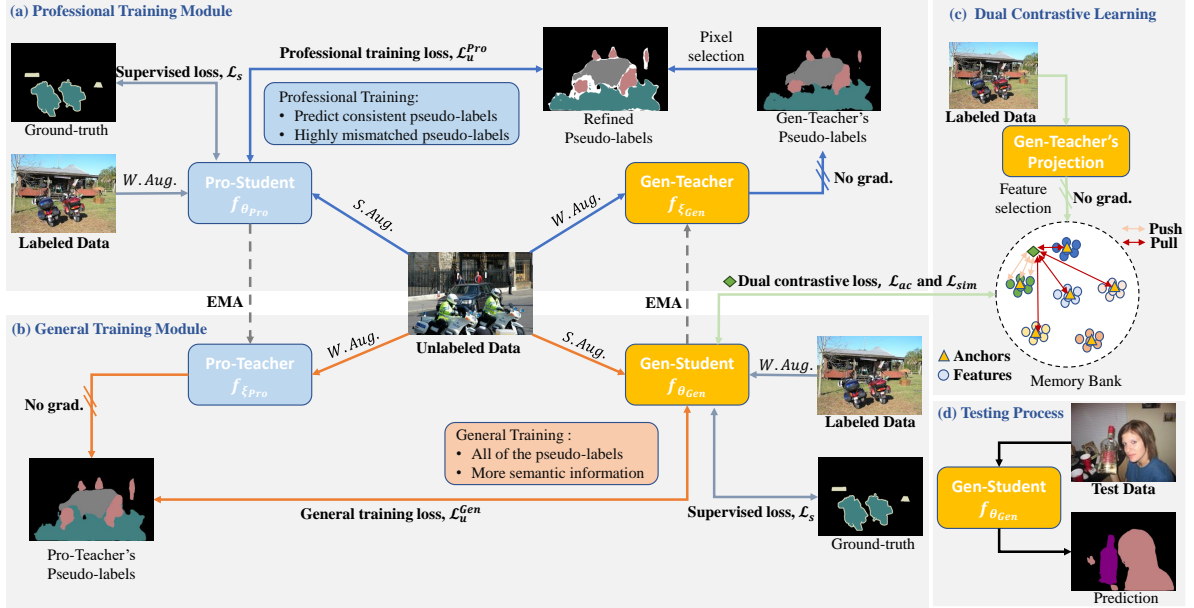


Fig. 3: Overview of our framework. For labeled images, we apply weak augmentation for a labeled image and then feed it into Gen-Student and Pro-Student, supervised by the ground truth. For unlabeled images, we use two different modules: (a) In the professional training module, we apply weak augmentation and strong augmentation to an unlabeled image, feeding them into Gen-Teacher and Pro-Student, respectively, and then use refined pseudo-labels by pixel selection from Gen-Teacher to supervise Pro-Student’s prediction. (b) In the general training module, weak and strong augmentations are applied to an unlabeled image, which are then fed into Pro-Teacher and Gen-Student, respectively, followed by the utilization of all pseudo-labels from Pro-Teacher to supervise Gen-Student’s prediction. (c) In addition, we introduce a dual contrastive learning to foster distinct decision boundaries in the model, ensuring that it does not solely cater to the majority classes. (d) We evaluate the performance of STPG using Gen-Student.

3.2 Synergistic Training

Overview. To mitigate the accumulation of erroneous knowledge during training and reduce coupling, we employ a dual mean teacher architecture alongside mutual learning. In this setup, the parameters of the teacher model in one module are updated through EMA using the student model in other module. Fig. 3 summarizes the overall framework and the training procedure. This framework consists of two parallel student models, Gen-Student $f_{\theta_{Gen}}$ and Pro-Student $f_{\theta_{Pro}}$, each with different initializations. Their corresponding teacher models are Gen-Teacher $f_{\xi_{Gen}}$ and Pro-Teacher $f_{\xi_{Pro}}$. Specifically, $f_{\theta_{Pro}}$ and $f_{\xi_{Gen}}$ form a professional training module, and $f_{\theta_{Gen}}$ and $f_{\xi_{Pro}}$ form a general training module, each focusing on a specific aspect. With the professional training module, Pro-Student and Pro-Teacher can

acquire more information from high-quality samples or from minority classes. In contrast, we hope that the general training module can learn more comprehensively.

Supervised Loss. For labeled images, as in most methods, a supervised loss is applied for Gen-Student and Pro-Student. Given the labeled image x_l and its corresponding label y_l , the supervised loss \mathcal{L}_s is written as:

$$\mathcal{L}_s = \ell_{ce}(f_{\theta_{Gen}}(\mathcal{A}^w(x_l)), y_l) + \ell_{ce}(f_{\theta_{Pro}}(\mathcal{A}^w(x_l)), y_l), \quad (1)$$

where $\mathcal{A}^w(\cdot)$ denotes weak data augmentation and ℓ_{ce} is the pixel-wise cross-entropy loss function.

Professional Training Module. The traditional learning approach tends to focus on majority classes and is not able to sufficiently learn

minority classes. Thus, we propose a pixel selection strategy for producing refined pseudo-labels to improve the performance. The loss is calculated using consistent and highly mismatched pseudo-labels from Gen-Teacher to supervise Pro-Student’s predictions instead of all the pseudo-labels.

For an unlabeled image, we obtain the prediction probabilities $p_u^{Pro}, \hat{p}_u^{Gen} \in [0, 1]^{W \times H \times C}$ from Pro-Student and Gen-Teacher and the pseudo-labels $\hat{y}_u^{Gen} \in \{0, 1\}^{W \times H \times C}$ from Gen-Teacher:

$$p_u^{Pro} = f_{\theta_{Pro}}(\mathcal{A}^s(x_u)), \quad (2)$$

$$\hat{p}_u^{Gen} = f_{\xi_{Gen}}(\mathcal{A}^w(x_u)), \quad (3)$$

$$\hat{y}_u^{Gen} = OneHot(\hat{p}_u^{Gen}), \quad (4)$$

where $\mathcal{A}^s(\cdot)$ and $\mathcal{A}^w(\cdot)$ denote strong augmentation and weak data augmentation, respectively. The function *OneHot* converts the probability into the one-hot format by assigning the most likely class for each pixel as one and the others as zero along the third axis of the matrix. Thus, only one entry along the third axis of each pixel in matrix \hat{y}_u^{Gen} can be one.

In this work, the pseudo-label represented by matrix \hat{y}_u^{Gen} are divided into three mutually exclusive parts: consistent pseudo-labels, highly mismatched pseudo-labels and low mismatched pseudo-labels, represented by \hat{y}_u^{Cons} , \hat{y}_u^{Hmis} , $\hat{y}_u^{Lmis} \in \{0, 1\}^{W \times H \times C}$. For each pixel along the third axis, only one of the three matrices can have a nonzero entry; namely, we can apply the following restriction: $\hat{y}_u^{Cons} + \hat{y}_u^{Hmis} + \hat{y}_u^{Lmis} = \hat{y}_u^{Gen}$.

Consistent pseudo-labels \hat{y}_u^{Cons} , as shown in Fig. 4(a), are defined as the pseudo-labels that both Gen-Teacher and Pro-Student have consistently predicted. Since the pixel predictions remain consistent across different training modules, we consider these pseudo-labels to be of high quality.

The highly mismatched pseudo-labels represented by \hat{y}_u^{Hmis} , as shown in Fig. 4(b), are computed in three steps.

(1) We construct the confusion matrix $M \in \mathbb{R}^{C \times C}$ with C as the number of classes for the predictions of Pro-Student and Gen-Teacher in each mini-batch. An illustration is shown in Fig. 5.

(2) We define a class-level mismatch score vector I by the confusion matrix, in which each

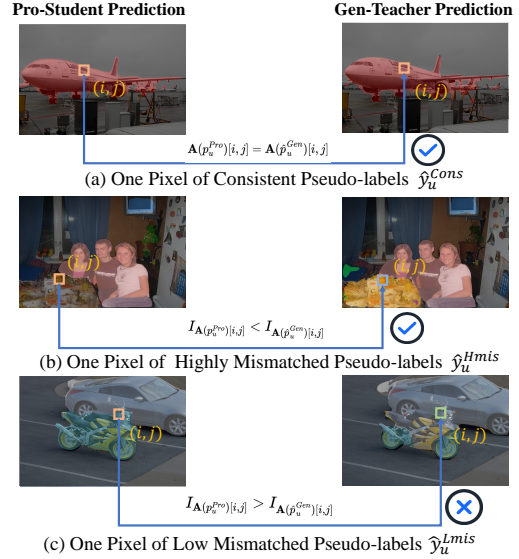


Fig. 4: Illustration of pixel selection strategy. $\mathbf{A}(\cdot)[i, j]$ represents the predicted class for the pixel located at the coordinates (i, j) . (a) When the two predictions of a pixel are consistent, they are used to train Pro-Student. (b) When the two predictions for a pixel are inconsistent, if the mismatch score of the class predicted by Gen-Teacher is larger than that of Pro-Student, the pixel usually contains more minority-class information and can be used for training Pro-Student. (c) Otherwise, these pseudo-labels are not used for training Pro-Student.

element represents the proportion of mismatched predictions of Pro-Student and Gen-Teacher for a certain class. For example, we compute the mismatch score of class q as follows:

$$I_q = \frac{\sum_{k=1}^C m_{q,k} - m_{q,q}}{\sum_{k=1}^C m_{q,k}} + \frac{\sum_{k=1}^C m_{k,q} - m_{q,q}}{\sum_{k=1}^C m_{k,q}}. \quad (5)$$

When it is large, this indicates a significant disagreement between the two models regarding Class q . This substantial disagreement suggests that Class q is likely a minority class. The reason is that these classes are more prone to being misclassified as other classes, which results in fewer pixels being assigned to them in the pseudo-labels compared to other classes. We map the class-level mismatch scores onto the pixel predictions of both the Pro-Student and Gen-Teacher to generate two mismatch matrices, denoted as $\mathbf{I}_{(\cdot)}$. These

		Gen-Teacher Predictions						
		C_1	...	C_p	...	C_q	...	C_C
Pro-Student Predictions	C_1	$m_{1,1}$...	$m_{1,p}$...	$m_{1,q}$...	$m_{1,C}$

	C_p	$m_{p,1}$...	$m_{p,p}$...	$m_{p,q}$...	$m_{p,C}$

	C_q	$m_{q,1}$...	$m_{q,q}$...	$m_{q,q}$...	$m_{q,C}$

C_C	$m_{C,1}$...	$m_{C,p}$...	$m_{C,q}$...	$m_{C,C}$	

■ Consistent ■ Mismatched

Fig. 5: Illustration of confusion matrix. For each batch, we compute the confusion matrix between the predictions of Gen-Teacher and those of Pro-Student to obtain a mismatch score for each class. For example, $m_{p,q}$ is the number of pixels where Pro-Student’s prediction is Class p and Gen-Teacher’s prediction is Class q ($p, q \in [1, 2, 3, \dots, C]$). The proportions of mismatched predictions in the orange boxes and yellow boxes indicate the mismatch scores for Class p and Class q , respectively.

matrices match the size of the image, with each element corresponding to the mismatch score of the predicted class, namely, $\mathbf{I}_{(\cdot)}[i, j] = I_{\mathbf{A}(\cdot)}[i, j]$. Here, $\mathbf{A}(\cdot)[i, j]$ represents the predicted class for the pixel located at the coordinates (i, j) and \cdot denotes p_u^{Pro} or \hat{p}_u^{Gen} .

(3) For inconsistent predictions between Pro-Student and Gen-Teacher, we select certain pseudo-labels to form highly mismatched pseudo-labels:

$$\hat{y}_u^{Hmis} = \hat{y}_u^{Gen} \times (\mathbf{I}_{(p_u^{Pro})} < \mathbf{I}_{(\hat{p}_u^{Gen})}), \quad (6)$$

where $\mathbf{I}_{(p_u^{Pro})} < \mathbf{I}_{(\hat{p}_u^{Gen})}$ is a binary matrix with each entry equal to one only if the mismatch score of the Gen-Teacher’s prediction is greater than the Pro-Student’s prediction for the corresponding pixel. For example, for a certain pixel, if the Pro-Student’s prediction is Class p and the Gen-Teacher’s prediction is Class q , and if $I_p < I_q$, we consider the Gen-Teacher’s prediction to be a highly mismatched pixel.

The low mismatched pseudo-labels \hat{y}_u^{Lmis} , as shown in Fig. 4(c), are the remaining pseudo-labels that do not belong to \hat{y}_u^{Cons} or \hat{y}_u^{Lmis} . These pseudo-labels are not used for training Pro-Student.

The professional training loss \mathcal{L}_u^{Pro} is computed as follows:

$$\mathcal{L}_u^{Pro} = \omega_u^{Pro} \ell_{ce}(p_u^{Pro}, \hat{y}_u^{Cons} + \hat{y}_u^{Hmis}), \quad (7)$$

where ω_u^{Pro} is a weighting matrix and each element of ω_u^{Pro} represents the confidence of a pseudo-label generated by the teacher model, i.e., $\omega_u^{Pro}[i, j] = \max_{c \in \{1, \dots, C\}} \hat{p}_u^{Gen}[i, j, c]$. For pseudo-labels not belonging to \hat{y}_u^{Cons} or \hat{y}_u^{Hmis} , the corresponding elements in ω_u^{Pro} are zero. Using the prediction confidence of the teacher model as the weight of the student model to calculate the loss can reduce the impact of suspicious noisy labels. Therefore, unlike traditional confidence thresholding approaches for filtering out numerous pseudo-labels, we can take advantage of unlabeled data.

General Training Module. For the general training module, we choose all pseudo-labels from Pro-Teacher as supervision for Gen-Student. For an unlabeled image, we obtain the prediction probability $p_u^{Gen}, \hat{p}_u^{Pro} \in [0, 1]^{W \times H \times C}$ from Gen-Student and Pro-Teacher and the pseudo-labels $\hat{y}_u^{Pro} \in \{0, 1\}^{W \times H \times C}$ from Pro-Teacher.

$$p_u^{Gen} = f_{\theta_{Gen}}(\mathcal{A}^s(x_u)), \quad (8)$$

$$\hat{p}_u^{Pro} = f_{\xi_{Pro}}(\mathcal{A}^w(x_u)), \quad (9)$$

$$\hat{y}_u^{Pro} = OneHot(\hat{p}_u^{Pro}), \quad (10)$$

The general training loss \mathcal{L}_u^{Gen} is calculated as follows:

$$\mathcal{L}_u^{Gen} = \omega_u^{Gen} \ell_{ce}(p_u^{Gen}, \hat{y}_u^{Pro}), \quad (11)$$

We similarly used the reweighting method mentioned above, and $\omega[i, j] = \max_{c \in \{1, \dots, C\}} \hat{p}_u^{Pro}[i, j, c]$

3.3 Dual Contrastive Learning with Anchors

Real-world datasets frequently display long-tail distributions, leading to significant class imbalances where dominant classes can distort model

training and influence decision boundaries for minority classes. To address this issue, we propose a dual contrastive learning with anchors. This strategy aims to maintain a uniform distribution of all classes, including minority classes, within the feature space. By doing so, it enhances decision boundaries and promotes better generalization, particularly effective for handling long-tailed data distributions.

Predefined Anchors. First, we define C as the number of classes and v_i with $i = 1, 2, 3, \dots, C$ as anchors. The dimension of each anchor is equal to the dimension of the features. These anchors are randomly initialized, and to ensure that each has the same distance as the others, we perform the following minimization approach: [42]:

$$\mathcal{L}_{Anchor} = \frac{1}{C} \sum_{i=1}^C \log \sum_{j=1}^C e^{v_i^T \cdot v_j / \tau}, \quad (12)$$

where τ is a temperature coefficient.

We also define c_i^t as the prototype of class i at time step t . To obtain the appropriate anchor for each class, we calculate the prototype of each class at the early stages of the training and iteratively update them by the EMA:

$$c_i^t = \alpha(c_i^{t-1}) + (1 - \alpha)(c_i^t), \quad (13)$$

where α is 0.99 by default to ensure that the prototypes were relatively stable. A prototype c_i is matched with the anchor index v_{σ_i} with the following constraints:

$$\sigma = \arg \min_{\sigma} \sum_{i=1}^C \|v_{\sigma_i} - c_i\|, \quad (14)$$

where σ is a distributive permutation of vector $[0, 1, 2, \dots, N]$ that represents a one-to-one correspondence between the class and the anchor. This optimization can be solved by the Hungarian algorithm [43].

Proximity-Guided Sampling. The memory bank stores representative features from labeled data and is used for contrastive learning [15, 25, 40]. Due to space limitations, the proposed memory bank only stores a subset of representative features obtained from labeled data, which comprises a first-in-first-out (FIFO) queue for each

class. Based on this, we propose a proximity-guided sampling strategy to obtain a more compact memory bank. We extract features only from Gen-Teacher by a projection head. To select the subset of features to be included in the memory bank, we predefine a threshold ϕ to choose the features with higher confidence, and then those features closer to their corresponding anchors are preferred. We update the memory bank only with the *top* – K closest features and pop out the outdated features at the top.

Dual Contrastive Loss. Traditionally, contrastive learning methods push features toward other features within the positive class and pull them away from others in negative classes. In our method, since features in the memory bank are selected to be close to their corresponding class anchor, we only need to keep features far away from the class anchors that they do not belong to, without needing exhaustive comparisons with all other features. We divide contrastive learning into two parts: anchor contrastive loss (\mathcal{L}_{ac}) and similarity loss (\mathcal{L}_{sim}).

Specifically, \mathcal{L}_{ac} brings the feature closer to its corresponding anchor while pushing it farther away from other anchors, forming uniform feature distributions. For each feature f , the corresponding class is c , which can be computed as follows:

$$\mathcal{L}_{ac} = -\log \frac{\exp(f \cdot v_{\sigma_c} / \tau)}{\exp(f \cdot v_{\sigma_c} / \tau) + \sum_{c' \in \sigma} \exp(f \cdot v_{\sigma_{c'}} / \tau)}, \quad (15)$$

where v_{σ_c} denotes the corresponding anchor of class c , and $v_{\sigma_{c'}}$ are other class anchors.

Additionally, \mathcal{L}_{sim} hopes that the features of the same class can be more compact.

$$\mathcal{L}_{sim} = \frac{1}{|M_c|} \sum_{i^+ \in Q_c} \left(1 - \frac{\langle f, i^+ \rangle}{\|f\|_2 \cdot \|i^+\|_2}\right), \quad (16)$$

where f represents the feature of the predicting pixel belonging to class c , i^+ denote the representative features of class c in the memory bank Q_c .

3.4 Training Process

In summary, the overall loss for each mini-batch is calculated as follows:

$$\mathcal{L}_{total} = \mathcal{L}_s + \lambda_u(\mathcal{L}_u^{Gen} + \mathcal{L}_u^{Pro}) + \lambda_{ctr}(\mathcal{L}_{ac} + \mathcal{L}_{sim}), \quad (17)$$

where \mathcal{L}_s represents supervised loss, \mathcal{L}_u^{Gen} is general training loss, \mathcal{L}_u^{Pro} is professional training loss, \mathcal{L}_{ac} stands for anchor contrastive loss, and \mathcal{L}_{sim} refers to similarity loss. The parameters λ_u and λ_{ctr} are weighting coefficients in the overall loss function.

4 Experimental Results

In this section, we assess the effectiveness of our proposed method on two well-established datasets: the Cityscapes dataset [44] and the PASCAL VOC 2012 dataset [45]. The experiments are performed using PyTorch on a server equipped with an NVIDIA A40 GPU.

4.1 Experimental Setting

Datasets. The Cityscapes dataset [44] is designed for semantic analysis of urban street scenes, includes 2975 training images with fine-grained annotations and 500 validation images, covering 19 classes. The PASCAL VOC 2012 dataset [45] serves as a standard benchmark for semantic segmentation with 20 object classes and 1 background class. It includes 1464 training images and 1449 validation images. Additionally, we use the SBD dataset [46] as an augmented set, which provides 9118 extra training images. Due to the coarse annotations in the SBD dataset, previous methods employ two primary partitioning strategies. The first strategy uses only the standard 1464 images as the entire labeled set, while the second strategy considers all 10582 images as potential labeled data. To ensure a fair comparison of our methods, we evaluate them using both a blender set (10582 potential labeled images) [15] and a classic set (1464 labeled images) [11].

Evaluation. To ensure a fair comparison with prior work, we use DeepLabv3+ [2] pretrained on ImageNet [47] as our segmentation model. The projection head for contrastive learning comprises a Conv-ReLU-Dropout-Conv block. The segmentation head and projection head map the ASPP

output to C classes and a 256-dimensional feature space, respectively. Consistent with previous studies, we evaluate segmentation performance using the mean intersection-over-union (mIoU) metric across all datasets. We utilize Gen-Student to evaluate the performance of our novel framework.

Implementation Details. The two student models share the same architecture, utilizing DeepLabV3+, but have different initializations. Both models are trained using the stochastic gradient descent (SGD) optimizer. When training on the Cityscapes dataset, the learning rate is initialized to 10^{-2} , whereas, for the PASCAL VOC 2012 dataset, it is 5×10^{-3} . The momentum for the optimizer is maintained at 0.9. For adjusting the learning rate, we employ a polynomial decay strategy defined by $1 - (\frac{\text{iter}}{\text{max_iter}})^{\text{power}}$, with the power parameter set to 0.9. During training, images are randomly cropped to 800×800 pixels with a batch size of 3 for the Cityscapes dataset. For the PASCAL VOC 2012 dataset, a crop size of 512×512 pixels with a batch size of 8 is used. The weights and hyperparameters for the loss functions are configured as follows: $\lambda_s = 1$, $\lambda_u = 1$, $\lambda_{ctr} = 0.1$, $\tau = 0.5$, $\phi = 0.95$, and $N = 256$. To implement strong data augmentation, three rectangular regions with random ratios ranging from 0.25 to 0.5 are randomly positioned within the input image and augmented using the CutMix [48] strategy.

4.2 Results

Results on the Cityscapes dataset. We evaluated the effectiveness of STPG using the Cityscapes dataset. To ensure fairness, DeepLabV3+ with ResNet50 is employed across all comparison methods. In all experiments, we arbitrarily choose 1/16, 1/8, and 1/4 of the Cityscapes training set as labeled data, corresponding to 186, 372, and 744 images respectively, with the remaining portion as unlabeled data. Table 1 presents the comparative results, where STPG demonstrates a substantial improvement over existing methods. Specifically, STPG enhances the mIoU by 8.03%, 8.40%, and 5.85% in the 1/16, 1/8, and 1/4 columns, respectively, compared to baseline methods using only labeled data.

Table 1: Comparisons of our STPG with the SOTA methods on the Cityscapes validation set using various partition protocols. We arbitrarily choose subsets from the training set of Cityscapes to use as labeled data: 1/16, 1/8, and 1/4, corresponding to 186, 372, and 744 images respectively, while the remaining training data serves as unlabeled. Each method employs **DeepLabV3+ with ResNet50**.

Methods	1/16 (186)	1/8 (372)	1/4 (744)
Sup. baseline	60.43	66.74	71.16
CAC [49]	-	69.7	72.7
PC ² Seg [41]	-	72.1	73.8
ELN [50]	-	70.3	73.5
ST++ [51]	-	72.7	73.8
PGCL [52]	-	71.2	73.9
MT [17]	66.1	72.0	74.5
CCT [21]	66.4	72.5	75.7
GCT [16]	65.8	71.3	75.3
MMFA [39]	66.2	73.6	76.9
STPG(Ours)	68.46	75.14	77.01

Results on the *blender* PASCAL VOC 2012 Dataset. We further assessed the performance of STPG on the blender PASCAL VOC 2012 dataset, ensuring all comparison methods utilized DeepLabV3+ with ResNet50 for consistency. In all experiments, we arbitrarily choose 1/16, 1/8, 1/4, and 1/2 of the PASCAL VOC 2012 training set as labeled data, corresponding to 662, 1323, 2646, and 5291 images respectively, with the remaining images treated as unlabeled data. Table 2 presents the comparative results. STPG consistently achieves state-of-the-art results across all partition protocols, surpassing existing best results by 0.08%, 0.19%, 1.17%, and 1.19% for the respective data splits.

Results on the *classic* PASCAL VOC 2012 Dataset. We evaluate STPG on the classic PASCAL VOC 2012 dataset by selecting labeled images from the original fine-grained annotated training set (1464 images total) and treating all images from the SBD as unlabeled data. For fairness, all comparative methods employed DeepLabV3+ with ResNet101. In all experiments, we arbitrarily choose 1/8, 1/4, 1/2, and the full set of the PASCAL VOC 2012 training data as labeled, corresponding to 183, 366, 732, and 1464 images respectively, with the remainder as unlabeled. Table 3 shows the comparison results.

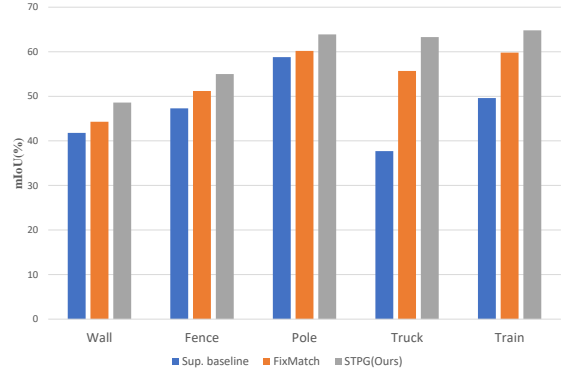


Fig. 6: Enhanced Performance for Tail Classes. The mIoU(%) for the tail classes (such as Wall, Fence, Pole, etc.) was evaluated using the baseline, FixMatch, and STPG. The results are derived from the Cityscapes dataset using 1/8 of the labeled data, employing DeepLabV3+ with ResNet50.

STPG consistently outperforms the supervised-only baseline, with improvements of +17.97%, +15.38%, +11.72%, and +8.33% for the 1/16, 1/8, 1/4, and 1/2 partition protocols, respectively.

Enhanced Performance for Tail Classes.

Due to the significant long-tail problem in the Cityscapes dataset, we conducted additional experiments on some of the tail classes (such as Wall, Fence and Pole, etc.) and compared STPG with the baseline and FixMatch [24]. As shown in Fig. 6, STPG can significantly improve the performance of the model on tail classes, thereby enhancing overall performance.

Comparison of T-SNE Visualization. We compare the data feature distributions produced by the baseline and STPG after T-SNE visualization. In Fig. 7, the features have been well-aligned and formed clusters by STPG. The model’s decision boundary becomes clearer, leading to more accurate predictions.

4.3 Analysis

In this section, we assess the performance improvements of proposed modules by conducting a series of experiments. These experiments use the Cityscapes and blender PASCAL VOC 2012 datasets, each with 1/8 of the data labeled. We utilize DeepLabV3+ with ResNet50 for all experiments.

Table 2: Comparisons of our STPG with the SOTA methods on the *blender* PASCAL VOC 2012 validation set using various partition protocols. We arbitrarily choose subsets from the PASCAL VOC 2012 training set to use as labeled data: 1/16, 1/8, 1/4, and 1/2, corresponding to 662, 1323, 2646, and 5291 images respectively, while the rest of the training set serves as unlabeled data. Each method employs **DeepLabV3+ with ResNet50**.

Methods	1/16 (662)	1/8 (1323)	1/4 (2646)	1/2 (5291)
Sup. baseline	61.72	66.83	71.52	73.96
CutMix-Seg [20]	68.9	70.7	72.5	74.5
ADS-SemiSeg [53]	-	70.8	72.8	-
ELN [50]	-	73.2	75.6	-
CPS [11]	72.0	73.7	74.9	76.2
ST++ [51]	72.6	74.4	75.4	-
U ² PL [15]	72.0	75.1	76.2	-
CPCL [54]	71.7	73.7	74.6	75.3
PGCL [52]	-	75.2	76.0	-
MMFA [39]	68.0	72.5	75.7	-
VC ^c [55]	73.8	75.3	75.8	-
STPG(Ours)	73.88	75.49	76.97	77.39

Table 3: Comparisons of our STPG with the SOTA methods on the *classic* PASCAL VOC 2012 validation set using different partition protocols. We arbitrarily choose subsets from the fine-grained annotated training set of PASCAL VOC 2012 to use as labeled data: 1/8, 1/4, 1/2, and the full set, corresponding to 183, 366, 732, and 1464 images respectively. The remaining training set, including all SBD images, serves as unlabeled data. Each method employs **DeepLabV3+ with ResNet101**.

Methods	1/8 (183)	1/4 (366)	1/2 (732)	Full (1464)
Sup. baseline	54.32	62.31	67.36	72.12
CutMix-Seg [20]	63.5	69.5	73.7	76.5
PseudoSeg [56]	65.5	69.1	72.4	73.2
PC ² Seg [41]	66.3	69.8	73.1	74.2
CPS [11]	67.4	71.7	75.9	-
CTT [25]	71.1	72.4	76.1	-
ST++ [51]	71.0	74.6	77.3	79.1
U ² PL [15]	69.2	73.7	76.2	79.5
PS-MT [57]	69.6	76.6	78.4	80.0
FPL [58]	71.7	75.7	79.0	-
PRCL [38]	74.4	76.7	-	78.2
STPG(Ours)	72.29	77.69	79.08	80.45

Ablation Studies. Table 4 presents the contributions of each module within our framework. Each module contributes significantly to enhancing semi-supervised semantic segmentation performance. Initially, the baseline \mathcal{L}_s , which is trained solely on labeled data, achieves a certain mIoU score. Then, we adopt the traditional mean-teacher architecture to introduce unlabeled data

\mathcal{L}_u and improve the performance of the model. However, the introduction of the dual mean teacher architecture (DM) individually boosts the mIoU to 73.37% for Cityscapes and 73.92% for PASCAL VOC 2012, indicating improvements of 6.63% and 7.09%, respectively.

Furthermore, incorporating the pixel selection strategy (PS) and dual contrastive learning (DCL)

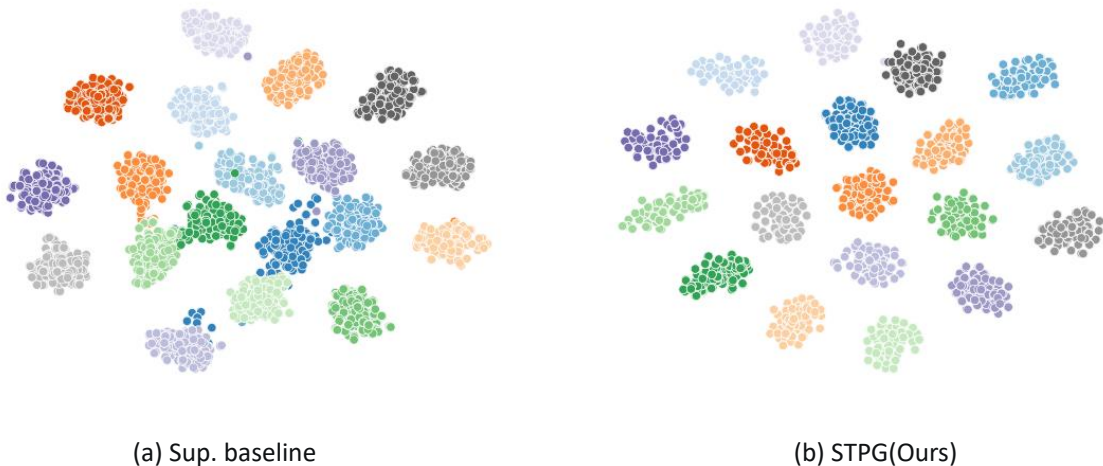


Fig. 7: Comparison of T-SNE Visualization. We use T-SNE to project features derived from the input data into a 2D space. For visualization, we sample 256 points per class. The resulting plot illustrates that STPG achieves superior clustering performance.

Table 4: Improvement of each proposed module: \mathcal{L}_s represents the supervised loss, while \mathcal{L}_u denotes the unsupervised loss. DM signifies a dual mean teacher architecture, PS denotes the pixel selection strategy, and DCL indicates dual contrastive learning. The results are obtained using 1/8 labeled data from both the Cityscapes and PASCAL VOC 2012 datasets, employing DeepLabV3+ with ResNet50.

					mIoU(%)	
\mathcal{L}_s	\mathcal{L}_u	DM	PS	DCL	Cityscapes	PASCAL VOC 2012
✓					66.74	66.83
✓	✓				72.10	72.63
✓	✓	✓			73.37	73.92
✓	✓	✓	✓		73.96	74.87
✓	✓	✓		✓	74.19	74.26
✓	✓	✓	✓	✓	75.14	75.49

modules leads to additional performance gains. The PS and DCL modules surpass the baseline by 7.22% and 7.45%, respectively, for Cityscapes and by 8.04% and 7.43%, respectively, for PASCAL VOC 2012.

Upon integrating these modules, the overall performance escalates, reaching 75.14% for Cityscapes and 75.49% for PASCAL VOC 2012. This comprehensive analysis underscores the effectiveness of the dual mean teacher architecture, pixel selection strategy, and dual contrastive learning in enhancing semi-supervised semantic segmentation.

Effect of Pixel Selection Strategy. As shown in Table 5, when all the settings are the same, selecting consistent and highly mismatched pseudo-labels yields the best performance. This finding indicates that highly mismatched pseudo-labels have a high probability of being correct once a prediction is made due to their difficulty in learning. In addition, because the two modules are different, if they are consistent on a pixel, there is a high probability that they will be correct.

Effect of the Memory Bank Size N . As illustrated in Fig. 8(a), the performance of the model is not significantly affected by variations

Table 5: Effect of pixel selection strategy. \hat{y}_u^{Cons} indicates pseudo-labels with consistency. \hat{y}_u^{Lmis} indicates low mismatched pseudo-labels. \hat{y}_u^{Hmis} indicates highly mismatched pseudo-labels. The results are derived from the Cityscapes dataset using 1/8 of the labeled data, employing DeepLabV3+ with ResNet50.

\hat{y}_u^{Cons}	\hat{y}_u^{Lmis}	\hat{y}_u^{Hmis}	mIoU(%)
✓			71.43
✓	✓		72.61
✓		✓	75.14
✓	✓	✓	73.56

in the size of the memory bank when other settings are kept constant. Minor adjustments to the memory bank size can result in slight changes in model performance. However, using an excessively large memory bank, such as a size of 512, may degrade performance. It’s important to note that setting $N = 0$ indicates the removal of contrastive learning from the framework. Since all features in the memory bank are utilized during the training, the computational load is directly proportional to the size N . To balance performance and computational efficiency, we have set the default memory bank size to 256.

Effect of Unsupervised Loss Weight λ_u .

In Fig. 8(b), we explore the effect of the unsupervised loss weight λ_u on the final segmentation performance. A weight of 0 indicates that the unlabeled data do not participate in training. The model is not sensitive to the unsupervised loss weight in a specific range and shows fluctuations while the overall performance is improved. The initial experiment involves setting the weight to 0.5, which resulted in an mIoU of 72.5%. Subsequently, we increase the weight to 1.0, placing equal emphasis on the unsupervised loss weight relative to the supervised loss weight. This adjustment leads to an improvement in the mIoU, achieving a value of 75.14%. Further exploration involves increasing the weight to 1.5, this adjustment yields a slightly lower mIoU of 73.94%.

4.4 Qualitative Results

Fig. 9 and Fig. 10 illustrate the qualitative results of STPG on the Cityscapes and PASCAL VOC 2012 datasets, respectively. Notably, our method

shows significant improvements over training with labeled data only, enhancing the performance of semi-supervised learning.

5 Conclusion

In this paper, we propose a new framework for semi-supervised semantic segmentation. The STPG framework with professional and general training modules can reduce model coupling and error accumulation and retain more semantic information for minority classes. Within the framework, a dual contrastive learning can alleviate the influence of majority class dominance in the feature space. Our approach is easily adaptable to various semi-supervised semantic segmentation networks. The experimental results show that STPG surpasses the state-of-the-art techniques.

Nevertheless, as with other semi-supervised learning approaches, the training process of our method is more time-consuming than that of fully supervised methods, and the correctness of pseudo-labels can greatly affect the effectiveness of contrastive learning, especially when features from different classes are similar in the feature space. Resolutions to these limitations can be explored in future studies.

Declarations

Authors contribution statement Yuting Hong: Conceptualization, Methodology, Software, Writing - Original Draft. **Hui Xiao:** Investigation. **Huazheng Hao:** Investigation. **Xiaojie Qiu:** Software, Writing - Review & Editing. **Baochen Yao:** Methodology, Software. **Chengbin Peng:** Conceptualization, Investigation, Methodology, Project Administration, Software, Writing - Original Draft, Funding acquisition, Resources, Writing - Review & Editing, Supervision.

Competing interests All the authors declare that they have no competing financial interests or personal relationships that could influence the work reported in this paper.

Ethical approval and consent to participate The work follows appropriate ethical standards in conducting research and writing the manuscript. This work presents computational models trained

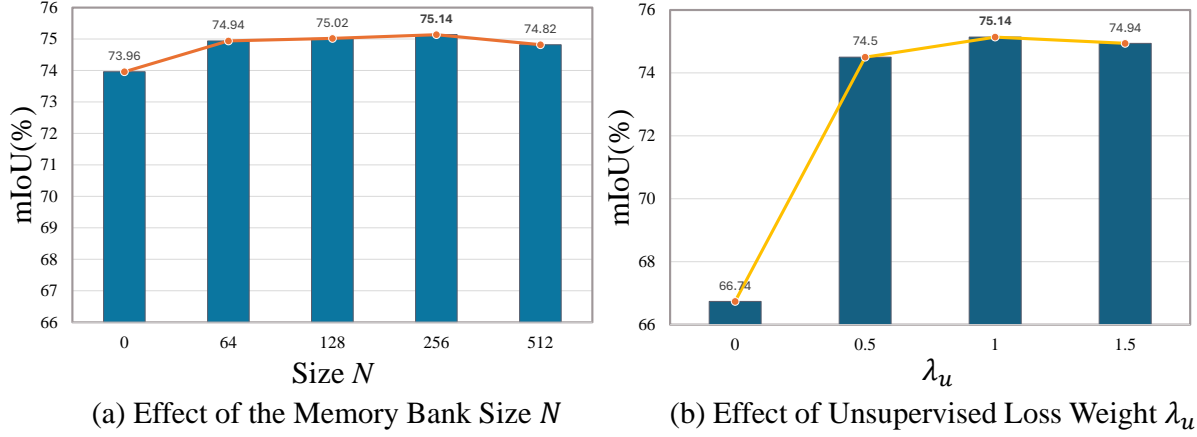


Fig. 8: Effect of hyper-parameters. (a) Effect of the memory bank size N ; (b) Effect of unsupervised loss weight λ_u . The results are derived from the Cityscapes dataset using 1/8 of the labeled data, employing DeepLabV3+ with ResNet50.

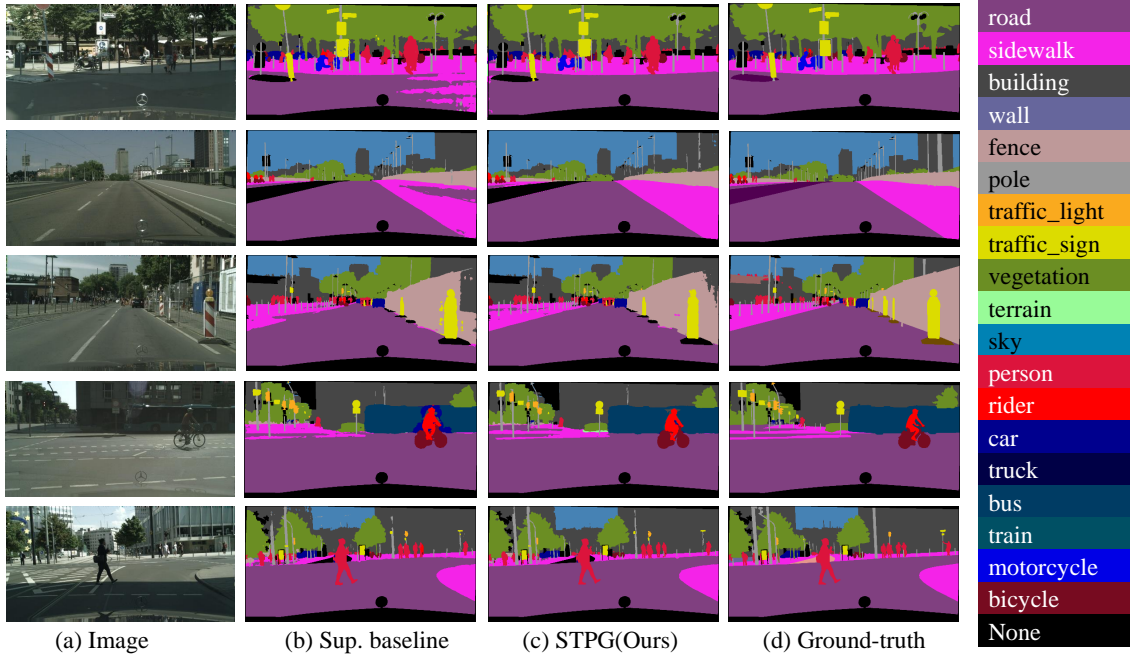


Fig. 9: Qualitative results of STPG framework using 1/8 labeled data from the Cityscapes training set. (a) Images from the validation set. (b) The results of training exclusively with labeled data. (c) The results achieved with STPG. (d) Ground-truths. All experiments are conducted using DeepLabV3+ with ResNet50.

with publicly available data, for which no ethical approval was required.

Data availability and access The data used to support the findings of this study is available from the corresponding author upon request.

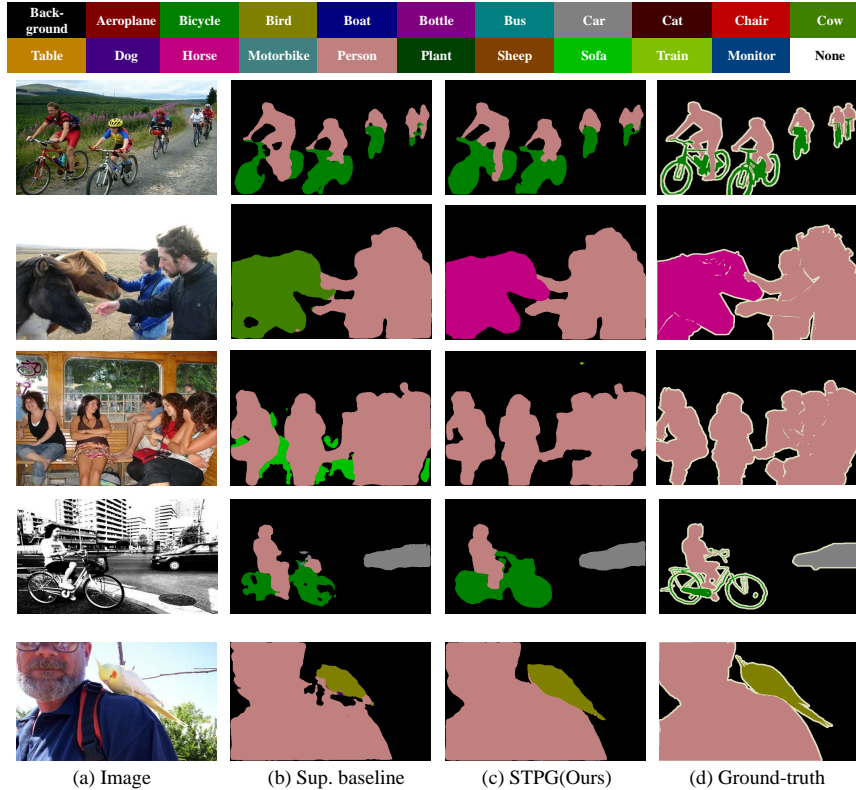


Fig. 10: Qualitative results of STPG framework using 1/8 labeled data from the PASCAL VOC 2012 training set. (a) Images from the validation set. (b) The results of training exclusively with labeled data. (c) The results achieved with STPG. (d) Ground-truths. All experiments are conducted using DeepLabV3+ with ResNet50.

References

- [1] Ji, J., Shi, R., Li, S., Chen, P., Miao, Q.: Encoder-decoder with cascaded crfs for semantic segmentation. *IEEE Transactions on Circuits and Systems for Video Technology* **31**(5), 1926–1938 (2020)
- [2] Chen, L.-C., Zhu, Y., Papandreou, G., Schroff, F., Adam, H.: Encoder-decoder with atrous separable convolution for semantic image segmentation. In: *Proceedings of the European Conference on Computer Vision*, pp. 801–818 (2018)
- [3] Xie, E., Wang, W., Yu, Z., Anandkumar, A., Alvarez, J.M., Luo, P.: Segformer: Simple and efficient design for semantic segmentation with transformers. *Advances in Neural Information Processing Systems* **34**, 12077–12090 (2021)
- [4] Huang, B., Zhu, Y., Usman, M., Chen, H.: Semi-supervised learning with missing values imputation. *Knowledge-Based Systems* **284**, 111171 (2024)
- [5] Peláez-Vegas, A., Mesejo, P., Luengo, J.: A survey on semi-supervised semantic segmentation. *arXiv preprint arXiv:2302.09899* (2023)
- [6] Badrinarayanan, V., Kendall, A., Cipolla, R.: Segnet: A deep convolutional encoder-decoder architecture for image segmentation. *IEEE transactions on pattern analysis and machine intelligence* **39**(12), 2481–2495 (2017)
- [7] Long, J., Shelhamer, E., Darrell, T.: Fully

- convolutional networks for semantic segmentation. In: Proceedings of the IEEE Conference on Computer Vision and Pattern Recognition, pp. 3431–3440 (2015)
- [8] Meng, F., Luo, K., Li, H., Wu, Q., Xu, X.: Weakly supervised semantic segmentation by a class-level multiple group cosegmentation and foreground fusion strategy. *IEEE Transactions on Circuits and Systems for Video Technology* **30**(12), 4823–4836 (2019)
- [9] Zhou, Q., Feng, Z., Gu, Q., Pang, J., Cheng, G., Lu, X., Shi, J., Ma, L.: Context-aware mixup for domain adaptive semantic segmentation. *IEEE Transactions on Circuits and Systems for Video Technology* (2022)
- [10] Zhao, Y., Zhong, Z., Luo, Z., Lee, G.H., Sebe, N.: Source-free open compound domain adaptation in semantic segmentation. *IEEE Transactions on Circuits and Systems for Video Technology* **32**(10), 7019–7032 (2022)
- [11] Chen, X., Yuan, Y., Zeng, G., Wang, J.: Semi-supervised semantic segmentation with cross pseudo supervision. In: Proceedings of the IEEE/CVF Conference on Computer Vision and Pattern Recognition, pp. 2613–2622 (2021)
- [12] Chen, J., Lu, W., Li, Y., Shen, L., Duan, J.: Adversarial learning of object-aware activation map for weakly-supervised semantic segmentation. *IEEE Transactions on Circuits and Systems for Video Technology* (2023)
- [13] Liao, M., Tian, S., Zhang, Y., Hua, G., Zou, W., Li, X.: Pda: Progressive domain adaptation for semantic segmentation. *Knowledge-Based Systems* **284**, 111179 (2024)
- [14] Hu, H., Wei, F., Hu, H., Ye, Q., Cui, J., Wang, L.: Semi-supervised semantic segmentation via adaptive equalization learning. *Advances in Neural Information Processing Systems* **34**, 22106–22118 (2021)
- [15] Wang, Y., Wang, H., Shen, Y., Fei, J., Li, W., Jin, G., Wu, L., Zhao, R., Le, X.: Semi-supervised semantic segmentation using unreliable pseudo-labels. In: Proceedings of the IEEE/CVF Conference on Computer Vision and Pattern Recognition, pp. 4248–4257 (2022)
- [16] Ke, Z., Qiu, D., Li, K., Yan, Q., Lau, R.W.: Guided collaborative training for pixel-wise semi-supervised learning. In: Proceedings of the European Conference on Computer Vision, pp. 429–445 (2020)
- [17] Tarvainen, A., Valpola, H.: Mean teachers are better role models: Weight-averaged consistency targets improve semi-supervised deep learning results. *arXiv preprint arXiv:1703.01780* (2017)
- [18] Ke, Z., Wang, D., Yan, Q., Ren, J., Lau, R.W.: Dual student: Breaking the limits of the teacher in semi-supervised learning. In: Proceedings of the IEEE/CVF International Conference on Computer Vision, pp. 6728–6736 (2019)
- [19] Bachman, P., Alsharif, O., Precup, D.: Learning with pseudo-ensembles. *Advances in neural information processing systems* **27** (2014)
- [20] French, G., Laine, S., Aila, T., Mackiewicz, M., Finlayson, G.: Semi-supervised semantic segmentation needs strong, varied perturbations. In: British Machine Vision Conference (2020)
- [21] Ouali, Y., Hudelot, C., Tami, M.: Semi-supervised semantic segmentation with cross-consistency training. In: Proceedings of the IEEE/CVF Conference on Computer Vision and Pattern Recognition, pp. 12674–12684 (2020)
- [22] Arazo, E., Ortego, D., Albert, P., O’Connor, N.E., McGuinness, K.: Pseudo-labeling and confirmation bias in deep semi-supervised learning. In: International Joint Conference on Neural Networks, pp. 1–8 (2020). IEEE
- [23] Lee, D.-H., *et al.*: Pseudo-label: The simple and efficient semi-supervised learning method for deep neural networks. In: Workshop on Challenges in Representation Learning, ICML, vol. 3, p. 896 (2013)

- [24] Sohn, K., Berthelot, D., Carlini, N., Zhang, Z., Zhang, H., Raffel, C.A., Cubuk, E.D., Kurakin, A., Li, C.-L.: Fixmatch: Simplifying semi-supervised learning with consistency and confidence. *Advances in neural information processing systems* **33**, 596–608 (2020)
- [25] Xiao, H., Li, D., Xu, H., Fu, S., Yan, D., Song, K., Peng, C.: Semi-supervised semantic segmentation with cross teacher training. *Neurocomputing* **508**, 36–46 (2022)
- [26] LeCun, Y., Bengio, Y., Hinton, G.: Deep learning. *nature* **521**(7553), 436–444 (2015)
- [27] Vaswani, A., Shazeer, N., Parmar, N., Uszkoreit, J., Jones, L., Gomez, A.N., Kaiser, L., Polosukhin, I.: Attention is all you need. *Advances in neural information processing systems* **30** (2017)
- [28] Cheng, B., Misra, I., Schwing, A.G., Kirillov, A., Girdhar, R.: Masked-attention mask transformer for universal image segmentation. In: *Proceedings of the IEEE/CVF Conference on Computer Vision and Pattern Recognition*, pp. 1290–1299 (2022)
- [29] Guo, M.-H., Lu, C.-Z., Hou, Q., Liu, Z., Cheng, M.-M., Hu, S.-M.: Segnext: Rethinking convolutional attention design for semantic segmentation. *Advances in Neural Information Processing Systems* **35**, 1140–1156 (2022)
- [30] Zheng, S., Lu, J., Zhao, H., Zhu, X., Luo, Z., Wang, Y., Fu, Y., Feng, J., Xiang, T., Torr, P.H., *et al.*: Rethinking semantic segmentation from a sequence-to-sequence perspective with transformers. In: *Proceedings of the IEEE/CVF Conference on Computer Vision and Pattern Recognition*, pp. 6881–6890 (2021)
- [31] Duan, Y., Zhao, Z., Qi, L., Wang, L., Zhou, L., Shi, Y., Gao, Y.: Mutexmatch: semi-supervised learning with mutex-based consistency regularization. *IEEE Transactions on Neural Networks and Learning Systems* (2022)
- [32] Kim, J., Min, Y., Kim, D., Lee, G., Seo, J., Ryoo, K., Kim, S.: Conmatch: Semi-supervised learning with confidence-guided consistency regularization. In: *European Conference on Computer Vision*, pp. 674–690 (2022). Springer
- [33] Chang, J.-H., Weng, H.-C.: Fully used reliable data and attention consistency for semi-supervised learning. *Knowledge-Based Systems* **249**, 108837 (2022)
- [34] Zhou, B., Lu, J., Liu, K., Xu, Y., Cheng, Z., Niu, Y.: Hypermatch: Noise-tolerant semi-supervised learning via relaxed contrastive constraint. In: *Proceedings of the IEEE/CVF Conference on Computer Vision and Pattern Recognition*, pp. 24017–24026 (2023)
- [35] Hu, Z., Yang, Z., Hu, X., Nevatia, R.: Simple: Similar pseudo label exploitation for semi-supervised classification. In: *Proceedings of the IEEE/CVF Conference on Computer Vision and Pattern Recognition*, pp. 15099–15108 (2021)
- [36] Chen, B., Jiang, J., Wang, X., Wan, P., Wang, J., Long, M.: Debaised self-training for semi-supervised learning. *Advances in Neural Information Processing Systems* **35**, 32424–32437 (2022)
- [37] Feng, Q., Xie, L., Fang, S., Lin, T.: Bacon: Boosting imbalanced semi-supervised learning via balanced feature-level contrastive learning. In: *Proceedings of the AAAI Conference on Artificial Intelligence*, vol. 38, pp. 11970–11978 (2024)
- [38] Xie, H., Wang, C., Zheng, M., Dong, M., You, S., Fu, C., Xu, C.: Boosting semi-supervised semantic segmentation with probabilistic representations. In: *Proceedings of the AAAI Conference on Artificial Intelligence*, vol. 37, pp. 2938–2946 (2023)
- [39] Yin, J., Zheng, Z., Pan, Y., Gu, Y., Chen, Y.: Semi-supervised semantic segmentation with multi-reliability and multi-level feature augmentation. *Expert Systems with Applications* **233**, 120973 (2023)
- [40] Alonso, I., Sabater, A., Ferstl, D., Montesano,

- L., Murillo, A.C.: Semi-supervised semantic segmentation with pixel-level contrastive learning from a class-wise memory bank. In: Proceedings of the IEEE/CVF International Conference on Computer Vision, pp. 8219–8228 (2021)
- [41] Zhong, Y., Yuan, B., Wu, H., Yuan, Z., Peng, J., Wang, Y.-X.: Pixel contrastive-consistent semi-supervised semantic segmentation. In: Proceedings of the IEEE/CVF International Conference on Computer Vision, pp. 7273–7282 (2021)
- [42] Wang, T., Isola, P.: Understanding contrastive representation learning through alignment and uniformity on the hypersphere. In: International Conference on Machine Learning, pp. 9929–9939 (2020). PMLR
- [43] Jonker, R., Volgenant, T.: Improving the hungarian assignment algorithm. *Operations Research Letters* **5**(4), 171–175 (1986)
- [44] Cordts, M., Omran, M., Ramos, S., Rehfeld, T., Enzweiler, M., Benenson, R., Franke, U., Roth, S., Schiele, B.: The cityscapes dataset for semantic urban scene understanding. In: Proceedings of the IEEE Conference on Computer Vision and Pattern Recognition, pp. 3213–3223 (2016)
- [45] Everingham, M., Van Gool, L., Williams, C.K., Winn, J., Zisserman, A.: The pascal visual object classes (voc) challenge. *International journal of computer vision* **88**, 303–338 (2010)
- [46] Hariharan, B., Arbeláez, P., Bourdev, L., Maji, S., Malik, J.: Semantic contours from inverse detectors. In: 2011 International Conference on Computer Vision, pp. 991–998 (2011). IEEE
- [47] Deng, J., Dong, W., Socher, R., Li, L.-J., Li, K., Fei-Fei, L.: Imagenet: A large-scale hierarchical image database. In: 2009 IEEE Conference on Computer Vision and Pattern Recognition, pp. 248–255 (2009). Ieee
- [48] Yun, S., Han, D., Oh, S.J., Chun, S., Choe, J., Yoo, Y.: Cutmix: Regularization strategy to train strong classifiers with localizable features. In: Proceedings of the IEEE/CVF International Conference on Computer Vision, pp. 6023–6032 (2019)
- [49] Lai, X., Tian, Z., Jiang, L., Liu, S., Zhao, H., Wang, L., Jia, J.: Semi-supervised semantic segmentation with directional context-aware consistency. In: Proceedings of the IEEE/CVF Conference on Computer Vision and Pattern Recognition, pp. 1205–1214 (2021)
- [50] Kwon, D., Kwak, S.: Semi-supervised semantic segmentation with error localization network. In: Proceedings of the IEEE/CVF Conference on Computer Vision and Pattern Recognition, pp. 9957–9967 (2022)
- [51] Yang, L., Zhuo, W., Qi, L., Shi, Y., Gao, Y.: St++: Make self-training work better for semi-supervised semantic segmentation. In: Proceedings of the IEEE/CVF Conference on Computer Vision and Pattern Recognition, pp. 4268–4277 (2022)
- [52] Kong, H., Lee, G.-H., Kim, S., Lee, S.-W.: Pruning-guided curriculum learning for semi-supervised semantic segmentation. In: Proceedings of the IEEE/CVF Winter Conference on Applications of Computer Vision, pp. 5914–5923 (2023)
- [53] Cao, C., Lin, T., He, D., Li, F., Yue, H., Yang, J., Ding, E.: Adversarial dual-student with differentiable spatial warping for semi-supervised semantic segmentation. *IEEE Transactions on Circuits and Systems for Video Technology* (2022)
- [54] Fan, S., Zhu, F., Feng, Z., Lv, Y., Song, M., Wang, F.-Y.: Conservative-progressive collaborative learning for semi-supervised semantic segmentation. *IEEE Transactions on Image Processing* (2023)
- [55] Hou, Y., Gould, S., Zheng, L.: View-coherent correlation consistency for semi-supervised semantic segmentation. *Pattern Recognition* **147**, 110089 (2024)

- [56] Zou, Y., Zhang, Z., Zhang, H., Li, C.-L., Bian, X., Huang, J.-B., Pfister, T.: Pseudoseg: Designing pseudo labels for semantic segmentation. *International Conference on Learning Representations* (2021)
- [57] Liu, Y., Tian, Y., Chen, Y., Liu, F., Belagiannis, V., Carneiro, G.: Perturbed and strict mean teachers for semi-supervised semantic segmentation. In: *Proceedings of the IEEE/CVF Conference on Computer Vision and Pattern Recognition*, pp. 4258–4267 (2022)
- [58] Qiao, P., Wei, Z., Wang, Y., Wang, Z., Song, G., Xu, F., Ji, X., Liu, C., Chen, J.: Fuzzy positive learning for semi-supervised semantic segmentation. In: *Proceedings of the IEEE/CVF Conference on Computer Vision and Pattern Recognition*, pp. 15465–15474 (2023)